Prediction of Turbulence Quantities for Swirling Flow in Conical Diffusers

Steven W. Armfield*
University of Western Australia, Western Australia, Australia
and
Nam-Hyo Cho† and Clive A. J. Fletcher‡
University of Sydney, Sydney, New South Wales, Australia

Turbulent swirling flow through 12 and 20 deg included angle diffusers, with moderate inlet swirl numbers sufficient to avoid wall flow separation, are predicted by a k-ϵ and an algebraic Reynolds stress turbulence model with a two-layer wall function. Good agreement with experimental data for the mean velocities and turbulence quantities is obtained by using an algebraic Reynolds stress turbulence model and a k-ϵ turbulence model with a suitable choice of the wall treatment. Both the amplification of the peak in turbulence quantitites and its increased distance from the diffuser wall, when compared to those of fully attached flow, are predicted very well for solid-body rotation swirling flow. The effect of different inlet swirl profiles on the flow behavior is also discussed.

I. Introduction

SWIRLING flow in confined geometries is an important subject because of its wide industrial use. The theory and modeling of turbulent swirling flows has been reviewed extensively by Gupta et al.[1] and Sloan et al.[2] Most attention has been given to strongly recirculating swirling flows in combustor geometries or free swirling jets. But swirling turbulent flow in diffusers also occurs in a number of commonly used fluid mechanical devices. For this reason many experiments have been performed to analyze which of the effects of swirl on the overall diffuser performance are important for efficient use,[3-5] but measurements of the turbulence quantities have not been undertaken very often. The industrial application of such devices makes it essential that accurate and economical predictions can be obtained for both the mean velocity field and the turbulence quantities.

In nonswirling diffuser flows, separation or near-separation is caused by the occurrence of a region of low axial momentum near the wall, because of the positive axial pressure gradient. It has been found that the inclusion of swirl upstream of the diffuser inlet can prevent separation occurring for diffuser angles and area ratios at which it would otherwise occur.[5]

As the flow passes into the diffuser, the turbulence quantities near the wall grow immediately downstream of the corner. As noted by Chieng and Launder,[6] for abrupt pipe expansion the region of high shear downstream of the corner is located further from the wall so that, for example, the generation rate of turbulent kinetic energy will exceed the dissipation rate, leading to the observed growth. Consequently, a significant local peak in all of the turbulence quantities occurs but displaced from the diffuser wall.

When solid-body rotation (SBR) swirl is present, the local peak in turbulence quantities occurs closer to the diffuser wall, and the radial gradients are more severe than in the nonswirling case.[7,8] In addition, further downstream, the local peaks in turbulence quantities diminish in magnitude. For all of these reasons, this is an important but difficult flow to compute accurately and is also a good test of alternative turbulence models.

Previous numerical predictions have been obtained using algebraic eddy-viscosity models, two-equation turbulence models, and algebraic Reynolds stress models (ASM) for swirling flow in conical diffusers with and without a tail pipe.[9-12] Okhio et al.[9] predicted the mean velocities in a 16.5 deg diffuser with a tail pipe using a Prandtl mixing length model. Armfield and Fletcher[10] provided the prediction for mean velocity field in a 7 deg diffuser using a reduced form of Navier-Stokes equations with a mixing length turbulence model. Habib and Whitelaw[11] calculated swirling recirculating flows using a k-ϵ turbulence model in wide-angle diffusers of 40 and 90 deg, with relatively longer tail pipes than the diffuser section. They compared the mean velocities and the turbulent kinetic energy with experimental data. Hah[12] used an algebraic Reynolds stress model to solve 8 and 16 deg diffuser flows, but it is very difficult to find predictions of the turbulence quantities for the practically important medium-angle diffusers, say 10 ~ 20 deg, without a tail pipe.

Recently, detailed measurements of turbulence quantities for a 20 deg swirling conical diffuser flow have been made by Clausen and Wood[8] in a complementary investigation to the present analysis. They found an optimum inlet SBR swirl level to give neither flow separation at the diffuser wall nor axial flow reversal at the centerline. This flow configuration is the major subject of the present computational investigation. A free-vortex (FV) inlet swirling flow through a 12 deg conical diffuser is also considered, but only mean flow (axial and swirl velocities) experimental results[5] are available with which to compare.

Results have been obtained using both the k-ϵ and ASM turbulence models, and the two models are compared in the present paper. The computational solutions and a consideration of a reduced form of the turbulent kinetic energy, k, transport equation provide a partial explanation (Sec. IV) for

Received June 2, 1988; revision received May 2, 1989.

*Research Fellow, Centre for Water Research.
†Research Assistant, Department of Mechanical Engineering. Member AIAA.
‡Reader, Department of Mechanical Engineering. Member AIAA.

the initial growth and subsequent axial decay of the near-wall peak in the turbulence quantities for an SBR swirling flow. An FV inlet swirling flow in a 12 deg conical diffuser[5] is predicted and compared with predictions for an SBR inlet swirling flow and a nonswirling flow in the same diffuser to assess the influence of the inlet swirl profile (Sec. III.B).

Two strategies to account for the near-wall viscous effects are available: the wall function method and the low-Reynolds-number modeling method.[13] Recently low-Reynolds-number modeling methods for computing full Reynolds stress closure have been used to apply the boundary conditions explicitly at solid walls,[14,15] but the wall function method with algebraic Reynolds stress or with full Reynolds stress closure has been widely used because of its computational efficienty. The sent study is a precursor for more complex fully three-dimensional flows where the greater economy of a wall function method will be decisive. However, it is expected that a near-wall, low-Reynolds-number modeling solution for the present problem would be as accurate but not so economical as the present approach. The results indicated in the present paper have been obtained using a two-layer wall function originally suggested by Chieng and Launder.[6] Such an approach is found to be more suitable for near-separating or separating flow than the simple mixing length formulation at near-wall grids.[16,17]

The layout of the rest of the paper is as follows. In Sec. II the governing equations, turbulence models, two-layer wall function, and the numerical scheme are described. Section III contains the results and a detailed description for an SBR inlet swirling flow, obtained with both the ASM and k-ϵ turbulence models. The significance of the results is discussed in Sec. IV, and the conclusions indicated in Sec. V.

II. Turbulence Models and Numerical Scheme

The mean flow k and ϵ and algebraic Reynolds stress equations[18] may be written in modeled form in terms of the mean velocity U, and the fluctuating velocity u, in coordinate free tensor form, as follows.

$$\rho U^j U^i_{,j} - \rho(\overline{\tau^{ij}})_{,j} = -g^{ij}P_{,j} + \mu g^{ij}U^i_{,lj} \tag{1}$$

$$U^i_{,i} = 0 \tag{2}$$

$$\underbrace{U^i k_{,i}}_{\text{convection}} = \underbrace{C_s\left[-(k/\epsilon)\tau^{ij}k_{,i}\right]_{,j}}_{\text{diffusion}} + P_k - \epsilon \tag{3}$$

$$\underbrace{U^i \epsilon_{,i}}_{\text{convection}} = \underbrace{C_\epsilon\left[-(k/\epsilon)\tau^{ij}\epsilon_{,i}\right]_{,j}}_{\text{diffusion}} + C_{\epsilon 1}(\epsilon/k)P_k - C_{\epsilon 2}\epsilon^2/k \tag{4}$$

$$(-\tau^{ij}/k)(P_k - \epsilon) = P^{ij} + \Phi^{ij} - \tfrac{2}{3}g^{ij}\epsilon \tag{5}$$

where P is the pressure, g is the metric tensor, μ is the dynamic viscosity and ρ is the density, and $\tau^{ij}(\equiv -\overline{u^i u^j})$ is the Reynolds stress tensor. Superscripts indicate contravariant quantities, subscripts indicate covariant quantities, and apostrophes in the lower position indicate covariant derivatives. The above equations are for a fluid with constant density and viscosity and are in the contravariant form.

In the algebraic Reynolds stress equations $P^{ij}(\equiv \tau^{ih}U^j_{,h} + \tau^{jh}U^i_{,h})$ represents production and Φ^{ij} is the pressure-strain term, modeled as[19-22]

$$\Phi^{ij} = \phi_1^{ij} + \phi_2^{ij} + \phi_{w1}^{ij} + \phi_{w2}^{ij} \tag{6}$$

where

$$\phi_1^{ij} = -C_1(\epsilon/k)(-\tau^{ij} - \tfrac{2}{3}g^{ij}k),\quad \phi_2^{ij} = -C_2(P^{ij} - \tfrac{2}{3}g^{ij}P_k) \tag{7}$$

$$\phi_{w1}^{ij} = C_1'(\epsilon/k)(-\tau^{nn}g^{ij} + 3/2\tau^{ni}g^{nj} + 3/2\tau^{nj}g^{ni})f(L/x_n) \tag{8}$$

$$\phi_{w2}^{ij} = C_2'(\phi_2^{nn}g^{ij} - 3/2\phi_2^{ni}g^{nj} - 3/2\phi_2^{nj}g^{ni})f(L/x_n) \tag{9}$$

$$f(L/x_n) = k^{3/2}/(C_w x_n \epsilon),\quad C_w = \kappa/C_\mu^{1/4} \tag{10}$$

The terms ϕ_1^{ij} and ϕ_2^{ij} model the degree of anisotropy of the turbulent kinetic energy and of the turbulent kinetic production, respectively. The "wall-echo terms," ϕ_{w1}^{ij} and ϕ_{w2}^{ij}, account for the increased anistropy due to the pressure reflection at the wall, f is the empirical wall damping coefficient to give unity in the near-wall region and a small value far from the wall, L is a turbulent length scale, and x_n is either the normal distance from the wall or the effective distance allowing for the global wall effect. The normal distance from the wall is used for x_n in this paper. The above wall-echo terms are expressed only for circular geometry such as a pipe or a diffuser.

When the k-ϵ turbulence model is used, the Boussinesq eddy-viscosity concept is applied as

$$\tau^{ij} = \nu_t(g^{jl}U^i_{,l} + g^{il}U^j_{,l}) - \tfrac{2}{3}g^{ij}k \tag{11}$$

The diffusion terms in the above k and ϵ equations are replaced with $g^{ij}[(\nu_{\text{eff}}/\sigma_k)k_{,i}]_{,j}$ and $g^{ij}[(\nu_{\text{eff}}/\sigma_\epsilon)\epsilon_{,i}]_{,j}$ respectively. The ν_{eff} is an effective viscosity equal to $\nu+\nu_t$, ν_t being the turbulent eddy viscosity defined as $\nu_t = C_\mu k^2/\epsilon$ and $\nu = \mu/\rho$ as the kinematic viscosity.

The constants used in the k-ϵ turbulence model are given the standard values commonly used: $C_\mu = 0.09$, $\sigma_k = 1.0$, $\sigma_\epsilon = 1.22$, $C_{\epsilon 1} = 1.44$, and $C_{\epsilon 2} = 1.92$. In the pressure-strain terms and the diffusion terms of the ASM turbulence model; the values are $C_1 = 1.8$, $C_2 = 0.6$, $C_1' = 0.5$, $C_2' = 0.3$, $C_s = 0.22$, and $C_\epsilon = 0.15$.[22,23]

In the present case we have chosen to use spherical coordinates as they conform naturally to the boundary of the physical domain and reduce flow-to-grid skewness when compared to Cartesian or cylindrical coordinate systems. Expressing the equations in physical spherical coordinates for a steady, incompressible, axisymmetric flow is a straightforward, though tedious, process. The detail expansions of all governing equations are provided by Armfield.[24]

A. Two-Layer Wall-Function

In the present investigation we wish to use the simplest possible turbulence model that will give a satisfactory prediction for the mean and turbulent fields in the class of swirling diffuser flow considered. Previously it has been found that use of an ASM turbulence model with a standard log-law wall function, or a modified mixing-length function in the wall region with the momentum equations integrated to the wall, has not provided satisfactory prediction of the turbulence quantities in the near-wall region, although the mean flow is well predicted.[24,25]

The two-layer near-wall formulation was proposed by Chieng and Launder[6] and developed by Viegas et al.[16] and Amano[17] to calculate separated and reattached flows. The turbulent kinetic energy at the first grid point away from the wall is calculated by the k-equation, Eq. (3), considering the effect of the viscous sublayer on the source terms, i.e., the mean generation and mean destruction rates of k, integrated over a cell extending from the wall to a point midway between the first and second grid points away from the wall. The convection and the diffusion terms in Eq. (3) are integrated also over the cell; obtained expressions are available in Refs. 17 and 26. In the present analysis the value of ϵ at the first grid point away from the wall is calculated by the local equilibrium condition.[6,16]

The assumed k and ϵ distributions are as follows.

In the viscous sublayer:

$$k = k_v\left(\frac{y}{y_v}\right)^2,\qquad \epsilon = 2\nu\left(\frac{\partial k^{1/2}}{\partial y}\right)^2 = 2\nu\frac{k_v}{y_v^2} \tag{12}$$

In the fully turbulent region:

$$k = ay + b = \left(\frac{k_2 - k_1}{y_2 - y_1}\right) y + k_1 - \left(\frac{k_1 - k_2}{y_1 - y_2}\right) y_1, \quad \epsilon = \frac{k^{3/2}}{\kappa y / C_\mu^{3/4}} \tag{13}$$

where κ is the von Kármán constant set to 0.41 and y is the distance from the wall. The edge of the viscous sublayer y_v is given by a universal value $Re_v (\equiv y_v k_v^{1/2}/\nu) = 20$, which is approximately $y^+ (\equiv y/\sqrt{\tau_w/\rho}) = 11.0$ for a local equilibrium condition. The distance y_v can be found from the above k distribution assumptions and Re_v.

Even though the above formulation is described here for a rectangular grid system, it can be applied easily to the spherical grid system used to obtain the results presented in Sec. III.

B. Boundary Conditions

The computational inflow boundary for SBR swirling flow[8] is set at station 2, $0.08D_0$ (D_0 = diameter of swirl generator section) downstream from the diffuser entrance, which is shown in Fig. 1. At the inflow boundary the axial velocity U, the radial velocity V, the swirl velocity W, and the turbulent kinetic energy k profiles are given by the experimental data (all variables are expressed in spherical coordinates hereafter). For the experimental FV swirling flow[5] only axial and swirl velocity profiles in cylindrical coordinates are available at entrance and exit so that radial velocity in cylindrical coordinates is set to zero at the inflow boundary, and k is taken as 0.5% of the inflow mean velocity energy.

The dissipation rate at the inflow boundary is obtained from the relation

$$\epsilon = C_\mu^{3/4} k^{3/2} / l \tag{14}$$

with $l = 0.01 D_0$, which leads to the correct axial k variation at the diffuser centerline. The remaining variables are assumed to have a constant axial gradient at the entrance.

From the axisymmetry of the flow the radial gradients of U, k, and ϵ are set to zero, and V and W are zero at the axis. The values of $\overline{v^2}$, $\overline{vw}$, and $\overline{uv}$ must be also specified at the axis due to the occurrence of the radial (θ) derivatives of $\overline{v^2}$, $\overline{vw}$, and $\overline{uv}$ in the momentum equations. From the experimental data[8,27] it seems reasonable to set $\overline{vw}$ and $\overline{uv}$ to zero, and the radial gradient of $\overline{v^2}$ to zero.

At the wall, no-slip boundary conditions for the velocity are implied. The turbulent kinetic energy, k, at the first grid point away from the wall is obtained from the k-equation with the modified wall treatment described in Sec. II.A with the assumption that $\partial k/\partial y = 0$ at the wall. The dissipation rate ϵ at the same point is obtained from the local equilibrium relation. All axial gradients are set to zero at the exit except for U. However, the axial gradient of UA is zero where A is the cross-sectional area. The normal gradient of the pressure, which is used as a boundary condition for the pressure equation, is set to zero on all boundaries, except the wall, where it is obtained directly by enforcing a mass-flow constraint.[24]

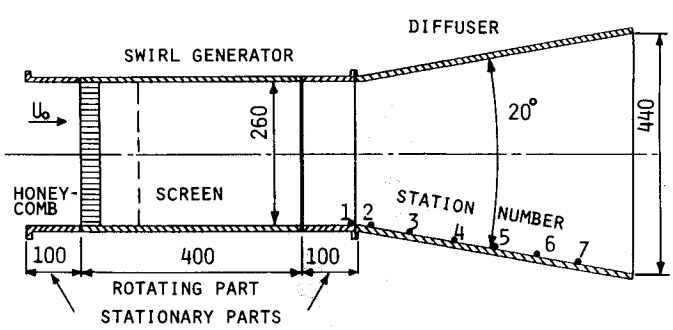

Fig. 1 Schematic diagram of swirl generator and diffuser. Axial positions for comparing with the experimental data are shown on the diffuser wall. All dimensions in mms.[8]

C. Numerical Scheme

To enable solutions to be obtained economically for the flow considered, a new finite-difference algorithm has been developed. The difficulty encountered is primarily because of the near-reversing axial velocity at the exit, coupled with the extremely low level of turbulence in the centerline region and large adverse pressure gradient, making the solution quite unstable. To counter this, a novel treatment of the pressure has been developed. Because of the focus of the present paper on the flow behavior, the numerical method is described elsewhere.[28]

Results presented in this paper have been obtained using a 40×40 grid system with a constant axial grid size and an exponentially stretched radial grid. The grid independency was checked using $20(x) \times 24(\theta) \sim 40(x) \times 60(\theta)$ grids. The 40×40 grid result for SBR swirling flow showed numerical errors in the mean flow quantities of less than 2% and in the near-wall peaks of turbulence quantities of less than 6% compared to those on a finer grid.

The first grid point away from the wall is located at $y^+ \approx 50$. The solution sensitivity to the location of the first grid point was tested for $y^+ = 30 \sim 100$. In this range the solution was relatively insensitive, especially for the near-wall peaks of the turbulence quantities (Figs. 4–8).

In the iterative procedure, relaxation factors are 0.4 for all nonturbulence quantities and 0.3 for the turbulence quantities. Convergence is assumed when the maximum change in any grid-point value of U between one iteration and the next is less than 1.0×10^{-4}. It is found that the variation of other variables is smaller than that of U, and the maximum residuals of the finite-difference equations are less than 0.5×10^{-3}. To ensure stable solutions with the ASM turbulence model, the k-ϵ turbulence model was used for the first $50 \sim 150$ iterations. Typically 500 iterations for the k-ϵ turbulence model and 800 iterations for the ASM turbulence model are required for convergence of SBR swirling flow. The CPU time for the ASM turbulence model solution on a Masscomp 5400 is of the order of 50 s per iteration for the 40×40 grid. The overall CPU time for the k-ϵ model is 70% of that for the ASM turbulence model.

III. Results

A. Solid-Body Rotation (SBR) Swirling Flow

In this section, predictions of mean flow and turbulence quantities are presented corresponding to the experimental results of Clausen and Wood.[8] The predicted results are obtained with both the ASM and k-ϵ turbulence models combined with the two-layer wall function.

The experimental data consists of radial distributions of mean velocities and turbulent Reynolds stresses at seven locations in a conical diffuser of 20 deg included angle with an area

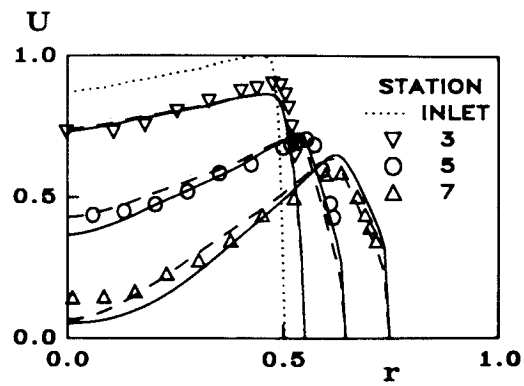

Fig. 2 Radial variation of axial velocity using ASM (———) and k-ϵ (– – – –) turbulence models. (same notation in Figs. 3–8). The inlet profile has same notation in Figs. 3 and 4).

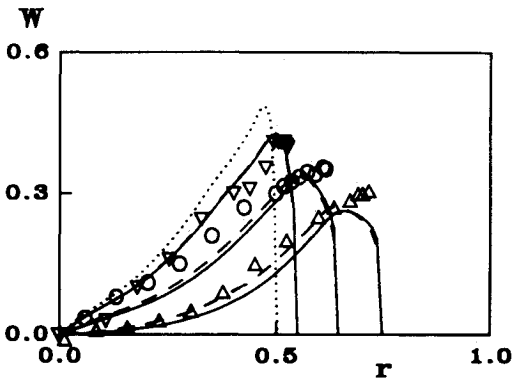

Fig. 3 Radial variation of swirl velocity.

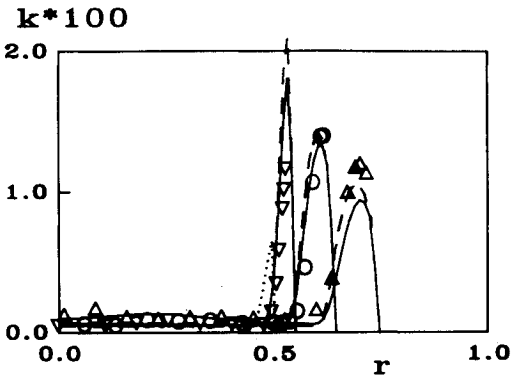

Fig. 4 Radial variation of turbulent kinetic energy.

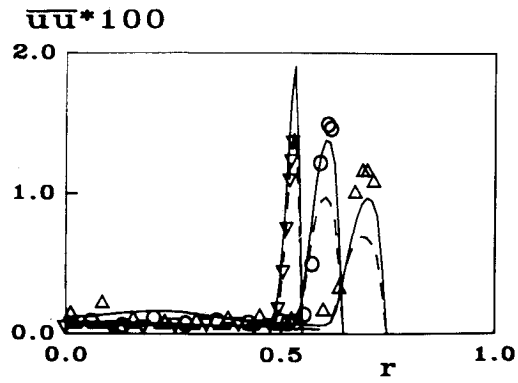

Fig. 5 Radial variation of Reynolds stress $\overline{u^2}$.

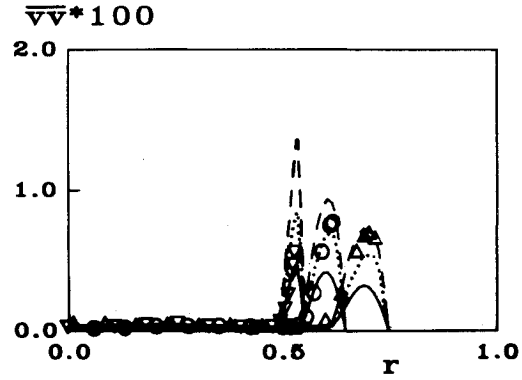

Fig. 6 Radial variation of Reynolds stress $\overline{v^2}$. The dotted line is for ASM without the wall-echo terms.

ratio of 2.84 at $Re = 212{,}000$ (Fig. 1). The diffuser angle is sufficient to cause boundary-layer separation in the absence of swirl. The swirl generator produces an inlet swirl profile of a solid-body rotation and close to uniform axial velocity in the core region. The detailed measurements were obtained for one inlet swirl distribution which led neither to separation at the wall nor centerline axial velocity reversal at the exit. The inlet swirl number is $SN[\equiv \int_0^R UWr^2\,dr/(R\int_0^R U^2 r\,dr)] = 0.25$. The experimental accuracy for the mean flow is within 6%.

Figure 2 shows the axial velocity profiles obtained by using the ASM and k-ϵ turbulence models and compared with the data of Clausen and Wood at three downstream locations (stations 3, 5, and 7 are at $xx = 0.28$, 0.83, and 1.40 from station 2 where xx is nondimensionalized by the diameter at station 2, Fig. 1). Both turbulence models predict reasonably the overall reduction in velocity associated with constant mass flow and the effect of swirl in reducing the centerline axial velocity and increasing the near-wall axial velocity. The centerline axial velocity is slightly underpredicted downstream.

The swirl velocity profiles are presented in Fig. 3. Both turbulence models predict accurately the solid-body rotation form at all axial locations in the core region, but underestimate the magnitude of the near-wall swirl velocity peak and predict that the influence of the wall causes a reduction in the swirl velocity further from the wall than is indicated by the experimental data. For both mean flow velocity components the ASM turbulence model predicts slightly lower values than the k-ϵ turbulence model in the core region.

Figure 4 displays the turbulent kinetic energy profiles. Both models predict quantitatively the magnitude and location of the turbulent kinetic energy peak near the wall and the flow characteristics, which double the magnitude of the turbulent kinetic energy peak downstream of the diffuser entrance corner. Further downstream the turbulent kinetic energy peak decays, which is consistent with the experimental results. Both turbulence models slightly underpredict the peak at the far downstream location and possibly overpredict in the near-entrance region. Because of the probe size, it is not evident from the experimental data how big the near-wall k peak is in the entrance region.

The $\overline{u^2}$ turbulent stress profiles are shown in Fig. 5. The ASM turbulence model predicts the magnitude of the near-wall peak very well but the k-ϵ turbulence model predictions are only 60% of the peak downstream value. Figure 6 shows the $\overline{v^2}$ turbulent stress profiles; the ASM turbulence model predicts only 50% of the peak level far downstream. However the ASM turbulence model solution includes substantial $\overline{v^2}$ damping associated with the pressure-strain "wall-echo" effect [Eqs. (8) and (9)]. When these terms are deleted, the dotted lines in Fig. 6, the agreement with the experimental data is much closer.

The experimental $\overline{w^2}$ profiles have near-wall peaks that are of comparable magnitude to the $\overline{v^2}$ near-wall peaks. Both turbulence models overpredict slightly (not shown) the $\overline{w^2}$ near-wall peaks.

Figure 7 presents the turbulent shear stress $\overline{uv}$ profiles. The ASM turbulence model underpredicts slightly the near-wall peak. In contrast the k-ϵ turbulence model gives good prediction downstream but may overpredict in the upstream region. The k-ϵ turbulence model produces a faster axial decay of maximum shear stress near the wall than does the ASM turbulence model. Both turbulence models indicate a very small sign reversal in $\overline{uv}$ at $r \approx 0.5$ that is not apparent in the experimental results. However the magnitude of the reversal is within the accuracy of the experimental data. The turbulent shear stress $\overline{vw}$ profiles are provided in Fig. 8. Both turbulence models underpredict the near-wall peak in the downstream region, and the k-ϵ turbulence model possibly overpredicts in the upstream region. As with the $\overline{uv}$ profiles, the k-ϵ turbulence model overestimates the rate of axial decay of the near-wall peak.

From the preceding results it can be seen that both turbulence models are giving reasonable solutions for the mean velocity components and the turbulence quantities, k and $\overline{uv}$. The magnitude and location of the near-wall peak in $\overline{u^2}$, produced by the ASM turbulence model, are reasonable. However although the predicted locations of the near-wall peaks in $\overline{v^2}$ and $\overline{w^2}$ are correct the predicted magnitudes do not indicate good agreement with the experimental data. This is primarily due to the modeling of the wall-echo effect, [Eqs. (8) and (9)] as will be indicated in Sec. IV.

B. Influence of Inlet Swirl Distribution

Senoo et al.[5] have investigated swirling conical diffuser flow with a free-vortex (FV) inlet swirl profile, an included diffuser angle of 12 deg with an area ratio of 4.0 and $Re = 300{,}000$. The FV inlet swirl number is $SN = 0.07$, and the experimental data consist of the radial distributions of U and W at entrance and exit ($xx = 0.0$, 5.0 respectively). No data for the turbulence quantities are available.

Figure 9 shows the axial velocity profiles at entrance and exit, predicted using the ASM turbulence model. The flow behavior predicted using the k-ϵ turbulence model (not shown) is very similar to that in Figs. 9 to 11. The radial distribution of the axial velocity is predicted reasonably but with slight underprediction near the wall and slight overprediction near the axis. This discrepancy may be caused by an inappropriate assumption of the inlet radial velocity distribution in cylindrical coordinates, which is difficult to estimate because of the dip in the axial velocity profile in the axis region. In the absence of any experimental data the inlet radial velocity components in cylindrical coordinates are set to zero.

The same U, V, and k profiles as those for the FV inlet swirling flow are used for the SBR inlet swirling flow, $SN = 0.20$, and for the nonswirling flow. As expected for an SBR inlet swirling flow, the swirl promotes a more rapid axial velocity decay in the core region than does the FV inlet swirling flow and increases the near-wall axial velocity, which tends to retard near-wall flow separation.

Figure 10 presents the swirl velocity profiles. The FV inlet swirl profile becomes flattened downstream, and this is predicted very well. The SBR inlet swirl profile is taken as a mirror image of the FV inlet swirl profile. The SBR swirl profile maintains its general form in the downstream direction, which is a similar behavior to that demonstrated in Fig. 3.

Figure 11 indicates the radial k distribution using the same inlet U, V, and k profiles for the three flow cases. The most remarkable difference between the SBR swirling flow and the others appears in the near-wall region. The near-wall peaks in k for the FV inlet swirling flow and the nonswirling flow (shown only at exit) are maintained at approximately the same level through the downstream extent of the diffuser, but, for the SBR inlet swirling flow, these decrease downstream consistent with the results shown in Fig. 4. We can assume the swirl component of FV inlet swirling flow is having little direct effect on the turbulence structure in the near-wall region from the evidence in Fig. 11 that, in this region, the inclusion of FV swirl changes k only a little. Clearly also the swirl component of SBR swirling flow is having a large effect in this region, acting to significantly damp the turbulence, which is to be expected.

The k level in the core region for FV inlet swirling flow increases up to 0.02 just downstream of the entrance region and decreases further downstream to the level shown in Fig. 11. The downstream k level for nonswirling flow is relatively lower than the others. But the rate of k variation in the core region in the downstream direction is slight, so that the present levels in the Fig. 11 are maintained for both nonswirling flow and SBR inlet swirling flow.

The k profile appears to correlate well with large radial gradients of the mean velocity components. In the near-axis

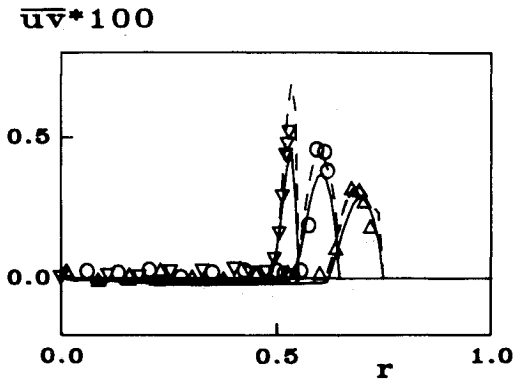

Fig. 7 Radial variation of Reynolds stress $\overline{uv}$.

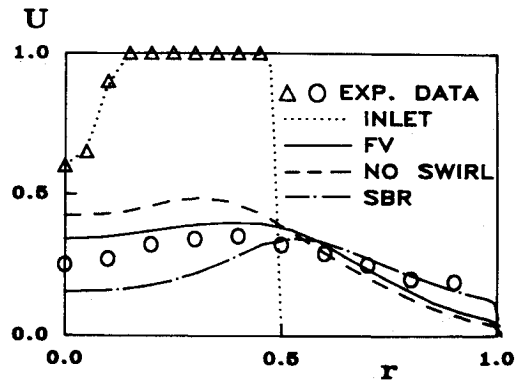

Fig. 9 Radial variation of axial velocity using ASM turbulence model (same notation as in Figs. 10 and 11).

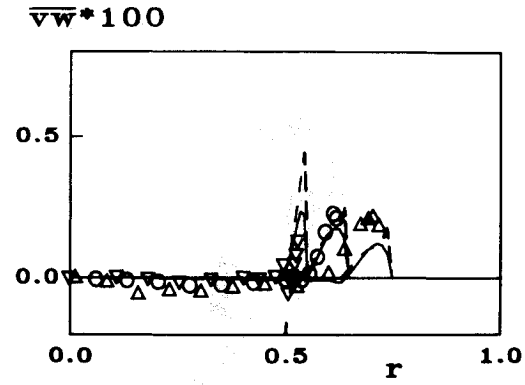

Fig. 8 Radial variation of Reynolds stress $\overline{vw}$.

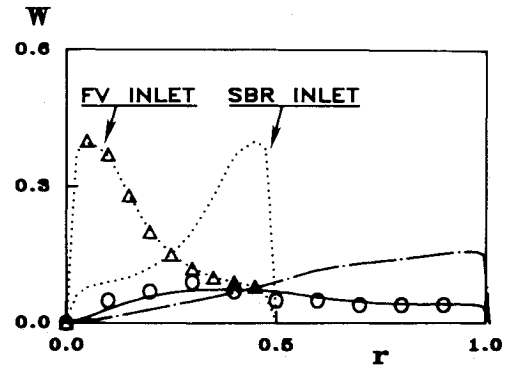

Fig. 10 Radial variation of swirl velocity.

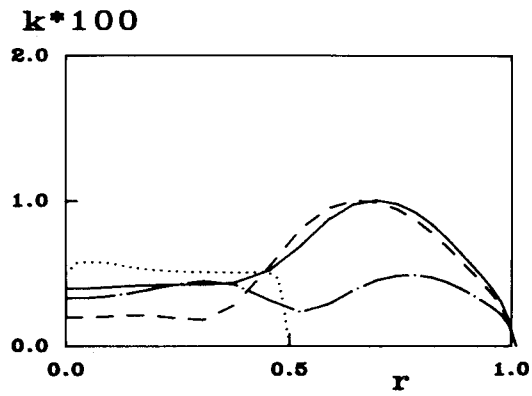

Fig. 11 Radial variation of turbulent kinetic energy.

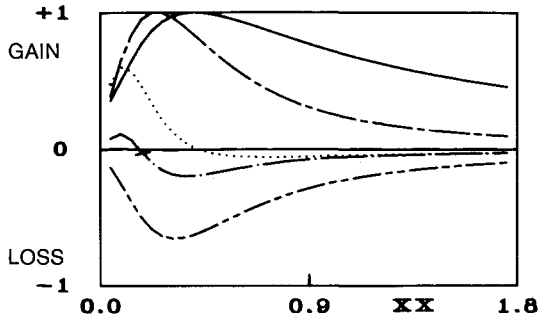

Fig. 12 Turbulent kinetic energy budget at the third grid point away from the wall along the axial direction; ——— k profile, —— - —— production, —— – – —— dissipation (negative), - · - · - · - radial diffusion, ····· axial convection.

region the FV swirling flow gives larger k values than the nonswirling flow because of larger gradients of mean velocity components leading to a significant production rate of k [e.g., second term in RHS of Eq. (16)]. Usually we expect that the k level for SBR swirling flow is lower than for nonswirling flow, because of the stabilizing effect of SBR swirl profile, particularly for the case of a uniform axial velocity component in the core region.[8] But in the present flow (Fig. 9) there is a big dip in the axial velocity in the core region so that stabilizing effect may be partly neutralized by the large radial gradient of the axial velocity components at intermediate downstream locations, giving magnitudes of k greater than for nonswirling flow. The downstream development of the individual nolds stresses follows similar trends as for k (Fig. 11).

IV. Discussion

Previously, satisfactory agreement with experimental measurements[8] of the mean flow has been achieved using an ASM turbulence model with a simple mixing length hypothesis to find k and ϵ in the near-wall region.[25] Despite the satisfactory computation of the mean velocities, relatively poor agreement for the turbulence quantities was obtained. In particular the large near-wall peak was not predicted accurately. As is demonstrated in the present paper, the use of the two-layer wall function has enabled good predictions of the turbulence quantities to be obtained as well as the mean velocity fields.

The following discussion is mainly concerned with the prediction of the Clausen and Wood flow.[8] As noted above, the ASM turbulence model underpredicts $\overline{v^2}$ (Fig. 6) and overpredicts $\overline{w^2}$ close to the wall, when plane-wall flow values of C_1' and C_2' are used in the wall-echo terms [Eqs. (8) and (9)]. We have also obtained solutions without the wall-echo terms in the ASM turbulence model. For the prediction of the mean velocities there is no difference between those two cases; for the normal stresses $\overline{u^2}$ there is a small difference. As shown in Fig.

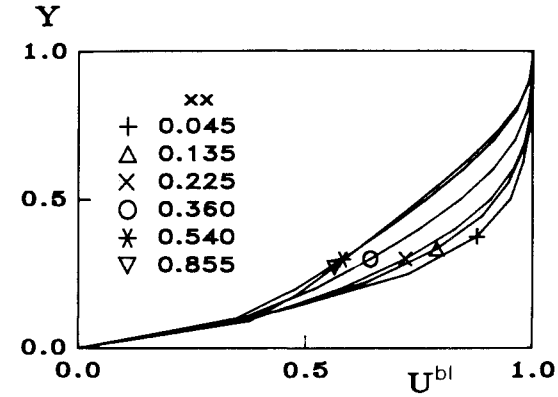

Fig. 13 Nondimensional axial velocity profiles in the boundary layer. Each symbol is located at the third grid point away from the wall of each profile at the axial position xx.

6, the ASM turbulence model without wall-echo terms predicts $\overline{v^2}$ better than the ASM turbulence model with wall-echo terms. This is also the case for $\overline{w^2}$ (not shown here). This implies that C_1' and C_2' could be tuned for a better fit but, in turn, this raises some concern about the universality of Eqs. (8) and (9). This is a potential weakness of the pressure-strain modeling. Different combinations of (C_1, C_2) in the pressure-strain term, Eqs. (6) and (7), were selected to test the sensitivity of the turbulence quantities prediction. The values (3.0, 0.3), suggested by Gibson and Younis[29] who showed good predictions for free swirling jet flows, did not show any difference in turbulence quantities prediction from that provided by the standard values (1.8, 0.6). This is not unexpected as the present flow is a confined swirling flow in which turbulence is produced mostly in the near-wall region rather than in the core region.

The turbulence quantities shown in Figs. 5–8 indicate an amplification of the near-wall peak in moving downstream from the diffuser entrance followed by a subsequent axial decay. This behavior may be partially explained by considering the turbulent kinetic energy budget. Figure 12 shows the axial variation of the turbulent kinetic energy budget based on Eq. (3) at a radial grid location near the wall. This is the approximate radial location at which the peak k occurs for the region downstream of the diffuser entrance. The various terms are shown in Fig. 12 by relative magnitude. It can be seen that both the production rate and the dissipation rate of k increase rapidly immediately downstream of the diffuser entrance but decay further downstream. The radial diffusion and the axial convection initially increase downstream of the diffuser entrance but become much smaller further downstream. The radial convection and the axial diffusion are very small throughout. Other turbulence quantities show a similar trend to that of k downstream of the diffuser entrance.

The behavior shown in Fig. 12 is discussed here in relation to the local reduced (i.e., retaining only dominant terms) k equation,

$$Uk_{,x} \simeq \left[\sin\theta(\nu_t/\sigma_k)k_{,\theta}\right]_{,\theta}/(x^2\sin\theta) + P_k - \epsilon \qquad (15)$$

The numerical results obtained with the ASM turbulence model indicate that, in the inner boundary layer, $-\overline{uv} \simeq \nu_t U_{,\theta}/x$ and $-\overline{vw} \simeq \nu_t[W_{,\theta}/x - W/(x\tan\theta)]$ so that Eq. (15) may be written as

$$Uk_{,x} \simeq \left[\sin\theta(\nu_t/\sigma_k)k_{,\theta}\right]_{,\theta}/(x^2\sin\theta) + \nu_t\left\{(U_{,\theta}/x)^2 + \left[W_{,\theta}/x - W/(x\tan\theta)\right]^2\right\} - C_\mu k^2/\nu_t \qquad (16)$$

The mean-flow behavior in the boundary layer downstream of the diffuser entrance has a similar character up to the point about $xx = 7\delta_0$ ($10\delta_0$ from the diffuser entrance corner), where

$\delta_0 (\approx 0.03 D_0)$ is the boundary-layer thickness at the diffuser entrance corner. For $xx \leq 7\delta_0$ the mean flow has a similar character as in the duct upstream of the diffuser and the boundary-layer edge is at a roughly constant distance from the diffuser centerline. This corresponds to a rapid growth in the boundary-layer thickness measured relative to the diffuser wall. At $xx \approx 7\delta_0$ the core region flow is first (in the downstream direction) influenced by the altered flow conditions emanating from the duct-diffuser wall junction. Under the combined influence of an adverse axial pressure gradient, swirl-driven radial pressure gradient and conservation of overall mass flow, the axial velocity component drops everywhere and the boundary-layer thickness grows at a slower rate, roughly linearly with x.

The nondimensional axial velocity profiles in the boundary layer are shown in Fig. 13 for various axial grid points downstream of the diffuser entrance. In Fig. 13, U^{bl} and Y are nondimensionalized by the axial velocity at the boundary-layer edge, i.e., the local maximum velocity, and the boundary-layer thickness. In the entrance region it can be seen that the profiles are almost similar so that a path with a constant radial value (as used in Fig. 12) corresponds to moving closer to the wall, in terms of Y. Thus $U_{,y}$ increases with xx up to $xx \approx 7\delta_0$. The turbulent eddy viscosity ν_t is roughly constant with x. The variation of $W_{,y}$ is similar to that of $U_{,y}$.

A consideration of Eq. (16) indicates that a growth in $U_{,y}$ and constant ν_t implies a rapid growth in the production rate, for $xx \leq 7\delta_0$, as is confirmed in Fig. 12. In turn this causes a growth in k [from Eq. (16)] and, as a result, a growth in the dissipation rate and the radial diffusion both tending to counteract the production rate. For $xx \geq 7\delta_0$ the reduction in the rate of the boundary-layer growth implies that a path with a constant radial value corresponds to an approximately constant Y in Fig. 13. The adverse pressure gradient is now more effective in retarding the mean axial flow leading to the flatter profiles in Fig. 13 and a fall in $U_{,y}$ at constant radial value. A consideration of Eq. (16) suggests that the production rate should fall, causing a reduction in k and ϵ as is confirmed in Fig. 12. The axial variation of k indicated in Fig. 12 has been explained above by examining the behavior of $U_{,y}$. This is not intended to imply that the $U_{,y}$ behavior *causes* the k variation.

The primary contributions of SBR swirl is to limit the rate of boundary-layer growth for $xx \geq 7\delta_0$ and to confine the physical effect of the turbulence to the region of the near-wall peak leading to much more severe radial gradients of the turbulence quantities than is found in nonswirling diffuser flows or in FV swirling diffuser flows.

It is expected that solid-body swirl distribution of the type in the Clausen and Wood flow[8] will stabilize the turbulence in the core region. This observed effect has led to the introduction of Richardson correction factors into the source terms of standard k-ϵ models, which are otherwise less satisfactory at predicting it.[2] Attempts to introduce a Richardson correction factor for swirling diffuser flow have not produced a significant improvement in the accuracy of the prediction.[25] It is considered that the use of an ASM turbulence model is a more satisfactory way of including this process than the introduction of Richardson correction factors, which tend to be highly empirical and coordinate-system dependent.

The present investigation indicates that both mean flow and turbulence quantities can be predicted accurately when a two-layer wall function is combined with a robust and accurate numerical algorithm. However, further improvement in the prediction of the precise Reynolds stress behavior is likely to depend on improved modeling of the pressure-strain terms, either in relation to the wall-echo terms used in an ASM turbulence model framework or by recourse to full Reynolds stress closure. For either approach the modeling of the ϵ equation is a potentially weak link.

The Clausen and Wood flow can be considered an extreme case of SBR type of swirling diffuser flow since any alternative degree of swirl for this diffuser will produce flow reversal. As the model gives good prediction for this case it is likely to give good prediction for less extreme examples of SBR swirling diffuser flow. Owing to the lack of detailed turbulence and mean flow measurements it has not been possible to perform a complete evaluation of the model for the FV swirling flow. Nonetheless the model has predicted the mean flow quite well. It seems likely that the algorithm developed is capable of giving accurate predictions of at least the mean flow quantities for a range of flows with inlet swirl profiles between the FV swirling flow of Senoo et al.[5] and the SBR swirling flow of Clausen and Wood.[8]

V. Conclusions

Good prediction of the mean and turbulence quantities in swirling flow has been obtained using an algebraic Reynolds stress turbulence model and a k-ϵ turbulence model with a two-layer wall function. The algebraic Reynolds stress turbulence model gives slightly better overall predictions of the turbulence quantities but is less robust computationally, requiring typically 60% more iterations to convergence. The use of a two-layer, rather than a single layer, wall function has been found to be necessary to predict accurately the level, location, and the axial variation of the near-wall peak in turbulence quantities for SBR swirl flow. The character of the near-wall peak is substantially different from that which occurs in either fully attached boundary layers, nonswirling, or FV inlet swirling diffuser flow. An SBR inlet swirling flow produces an increased near-wall axial velocity and decreased near-axis velocity compared with an FV inlet swirling flow and much more severe radial gradients of the near-wall turbulence quantities. Without modification the algorithm gives good prediction of the mean flow quantities in free vortex type swirling diffuser flow, a fundamentally different type of flow from the solid-body rotation flow of Clausen and Wood. Further evaluation of the model for free vortex flow will require a more detailed set of turbulence measurements.

Acknowledgment

The authors are grateful to the Australian Research Grants Committee for the support given to this research.

References

[1]Gupta, A. K., Lilley, D. G., and Syred, N., *Swirl Flows,* Abacus, Kent, England, UK, 1984.

[2]Sloan, D. G., Smith, P. J., and Smoot, L. D., "Modeling of Swirl in Turbulent Flow Systems," *Progress Energy Combustion Sciences,* Vol. 12, No. 3, 1986, pp. 163–250.

[3]So, K. L., "Vortex Phenomena in a Conical Diffuser," *AIAA Journal,* Vol. 5, June 1967, pp. 1072–1078.

[4]McDonald, A. T., Fox, R. W., and Van Dewoestine, R. V., "Effects of Swirling Inlet Flow on Pressure Recovery in Conical Diffusers," *AIAA Journal,* Vol. 9, Oct. 1971, pp. 2014–2018.

[5]Senoo, Y., Kawaguchi, N., and Negata, T., "Swirl Flow in Conical Diffusers," *Bulletin of the Japanese Society of Mechanical Engineers,* Vol. 21, No. 151, 1978, pp. 112–119.

[6]Chieng, C. C. and Launder, B. E., "On the Calculation of Turbulent Heat Transport Downstream from an Abrupt Pipe Expansion," *Numerical Heat Transfer,* Vol. 3, No. 2, 1980, pp. 189–207.

[7]Okwuobi, P. A. C. and Azad, R. S., "Turbulence in a Conical Diffuser with Fully Developed Flow at Entry," *Journal of Fluid Mechanics,* Vol. 57, Pt. 3, 1973, pp. 603–622.

[8]Clausen, P. D. and Wood, D. H., "Some Measurements of Swirling Flow through an Exisymmetric Diffuser," *Proceedings of Sixth Symposium on Turbulent Shear Flows,* edited by F. J. Durst et al., Paul Sabatier Univ., Toulouse, France, Sept. 7–9, 1987, pp. 1.3.1–1.3.5.

[9]Okhio, C. B., Horton, H. P., and Langer, G., "The Calculation of Turbulent Swirling Flow through Wide Angle Conical Diffusers and the Associated Dissipative Losses," *International Journal of Heat and Fluid Flow,* Vol. 7, No. 1, March 1986, pp. 37–48.

[10]Armfield, S. W. and Fletcher, C. A. J., "Numerical Simulation of Swirling Flow in Diffusers," *International Journal for Numerical Methods in Fluids,* Vol. 6, 1986, pp. 541–556.

[11]Habib, M. A. and Whitelaw, J. H., "The Calculation of Turbulent Flow in Wide-angle Diffusers," *Numerical Heat Transfer,* Vol. 5, No. 2, 1982, pp. 145–164.

[12]Hah, C., "Calculation of Various Diffuser Flows with Inlet Swirl and Inlet Distortion Effect," *AIAA Journal,* Vol. 21, Aug. 1983, pp. 1127–1133.

[13]Launder, B. E. and Spalding, D. B., "The Numerical Computation of Turbulent Flows," *Computational Methods in Applied Mechanics and Engineering,* Vol. 3, 1974, pp. 269–289.

[14]So, R. M. C. and Yoo, G.-J., "Low Reynolds Modeling of Turbulent Flows With and Without Wall Transpiration," *AIAA Journal,* Vol. 25, Dec. 1987, pp. 1556–1564.

[15]Shima, N., "A Reynolds-stress Model for Near-Wall and Low-Reynolds-Number Regions," *Transaction of the ASME, Journal of Fluids Engineering,* Vol. 110, March 1988, pp. 38–44.

[16]Viegas, J. R., Rubesin, M. W., and Horstman, C. C., "On the Use of Wall Functions as Boundary Conditions for Two-Dimensional Separated Compressible Flows," AIAA Paper 85-0180, Jan. 1985.

[17]Amano, R. S., "Development of a Turbulence Near-Wall Model and its Application to Separated and Reattached Flows," *Numerical Heat Transfer,* Vol. 7, No. 1, 1984, pp. 59–75.

[18]Rodi, W., "A New Algebraic Relation for Calculating the Reynolds Stresses," *Zeitschrift für Angewandte Mathematik und Mechanik,* Vol. 56, 1976, pp. 219–221.

[19]Launder, B. E., Reece, G. J., and Rodi, W., "Progress in the Development of a Reynolds Stress Turbulence Closure," *Journal of Fluid Mechanics,* Vol. 68, Pt. 3, 1975, pp. 537–566.

[20]Naot, D., Shavit, A., and Wolfshtein, M., "Interactions Between Components of the Turbulent Velocity Correlation Tensor due to Pressure Fluctuations," *Israel Journal of Technology,* Vol. 8, No. 3, 1970, pp. 259–269.

[21]Shir, C. C., "A Preliminary Numerical Study of Atmospheric Turbulent Flows in the Idealized Planetary Boundary Layer," *Journal of Atmospheric Sciences,* Vol. 30, Oct. 1973, pp. 1327–1339.

[22]Gibson, M. M. and Launder, B. E., "Ground Effects on Pressure Fluctuations in Atmospheric Boundary Layer," *Journal of Fluid Mechanics,* Vol. 86, Pt. 3, April 1978, pp. 491–511.

[23]Launder, B. E. and Morse, A., "Numerical Prediction of Axisymmetric Free Shear Flows with a Reynolds Stress Closure," *Turbulent Shear Flows 1,* edited by F. Durst, B. E. Launder, F. W. Schmidt, and J. H. Whitelaw, Springer-Verlag, Berlin, Heidelberg, New York, 1979, pp. 279–294.

[24]Armfield, S. W., "Numerical Simulation of Incompressible Turbulent Swirling Flow in Conical Diffusers," Ph.D. Thesis, University of Sydney, Sydney, Australia, 1987.

[25]Armfield, S. W. and Fletcher, C. A. J., "Comparison of k-ϵ and Algebraic Reynolds Stress Models for Swirling Diffuser Flow," *International Journal for Numerical Methods in Fluids,* Vol. 9, No. 8, 1989, pp. 987–1009.

[26]Johnson, R. W., "Turbulent Convection Flow in a Square Duct with a 180° Bend; an Experimental and Numerical Study," Ph.D. Thesis, University of Manchester, Manchester, England, UK, 1984.

[27]Sislian, J. P. and Cusworth, R. A., "Measurements of Mean Velocity and Turbulence Intensities in a Free Isothermal Swirling Jet," *AIAA Journal,* Vol. 24, Feb. 1986, pp. 303–309.

[28]Armfield, S. W. and Fletcher, C. A. J., "A Multi-sweep Scheme for Internal Turbulent Flows," 1989, submitted for publication.

[29]Gibson, M. M. and Younis, B. A., "Calculation of Swirling Jets with a Reynolds Stress Closure," *Physics of Fluids,* Vol. 29, No. 1, Jan. 1986, pp. 38–48.